

Article

Study on Static Strain Aging Kinetics of High-Carbon Steel Wires and Its Impact on High-Strength Steel Cords

Tamás Bálint Mező ^{*}  and Péter Barkóczy 

Institute of Physical Metallurgy, Metal Forming and Nanotechnology, University of Miskolc, 3515 Miskolc, Hungary; fembarki@uni-miskolc.hu

^{*} Correspondence: tamas.mezo81@gmail.com; Tel.: +36-202-122-822

Abstract: Under quasi-static loading, an irregular failure mode of high-strength thin carbon steel cords were observed after low-temperature thermal aging. Character and kinetics of damage in such wire ropes highly depend on the plastic elongation of the steel wires, which is significantly modified by the strain aging effect. In this paper, the static strain aging effect on heavily drawn high-carbon steel wires and their cords is experimentally studied in the 80–200 °C temperature range. The kinetics of the aging process is studied in detail. Experimental data are fit by the Johnson–Mehl–Avrami–Kolmogorov (JMAK) kinetic model. The temperature dependence of the static strain aging process is given by means of the Arrhenius equation. The associated JMAK exponents, the apparent activation energy and the pre-exponential constant are determined. Quantitative analysis of the affected strength and strain parameters is given, and based on this, the macroscopic failure mechanism is fundamentally explained.

Keywords: strain aging; kinetics; Avrami; drawn steel wire; wire rope; steel cord



Citation: Mező, T.B.; Barkóczy, P. Study on Static Strain Aging Kinetics of High-Carbon Steel Wires and Its Impact on High-Strength Steel Cords. *Metals* **2021**, *11*, 1684. <https://doi.org/10.3390/met11111684>

Academic Editors: João Pedro Oliveira, Eric D. van Hullebusch, Belén Díaz Fernández, Leszek Adam Dobrzański, Jae-chun Lee and Alex Lanzutti

Received: 30 September 2021
Accepted: 20 October 2021
Published: 22 October 2021

Publisher's Note: MDPI stays neutral with regard to jurisdictional claims in published maps and institutional affiliations.



Copyright: © 2021 by the authors. Licensee MDPI, Basel, Switzerland. This article is an open access article distributed under the terms and conditions of the Creative Commons Attribution (CC BY) license (<https://creativecommons.org/licenses/by/4.0/>).

1. Introduction

High-pressure flexible pipes are a unique field of application of high-strength carbon steel wires and strands made of them. These reinforcement plies are embedded in rubber and give the primary strength of the composite hose structure while they keep its flexibility (Figure 1). These pipes are typically used in the oil and gas industry, where extreme high pressure—up to 300 MPa—is common [1]. Designing flexible structures to such mechanical loads is challenging and highly based on proper information about the mechanical characteristics of the steel strands, especially their tensile properties. Because of the extraordinary conditions, any phenomena that may affect the mechanical behavior of the steel plies must be known and studied in detail [2].



Figure 1. Typical structure of a high-pressure oil hose [1].

Depending on the reinforcement cord type, they may consist of wires of the same, or different diameters. The characteristics of the strands are determined by the properties of the individual wires as well as the stranding parameters like the layer construction, the number of wires, lay lengths and lay directions [3]. The primary design parameters that are generally considered are the ultimate tensile strength, yield strength, elongation at break, and the apparent elastic modulus of the wire ropes. Appropriate determination of these values assures the safe operation of the rubber hoses up to the highest standards of the hazardous oil industry.

The wires are made of high carbon (0.8–0.9 wt.%) steel. Their high strength originates in the fine pearlitic structure and the recurring cold deformation during the drawing process. The ultimate tensile strength of these wires exceeds 2000 N/mm². Strain aging is a natural process in steel that has previously experienced cold deformation. It results in a further increase in tensile strength. On the other hand, it significantly decreases elongation [4,5].

The phenomenon of strain aging of steel has been intensively researched for decades. The basic principle of the process is now widely accepted. The cold plastic deformation generates dislocations in the considerably deformed metallic lattice [6]. The increased number of lattice defects initially causes significant ductility of the material. Elements that are interstitially present, mainly carbon in this case, diffuse into the affected zone and interact with the dislocations. In this way, the further movement of the dislocations becomes obstructed [4]. Carbon diffusion in steel is a relatively slow process. Thus, strain aging requires time [7].

In the literature, two forms of strain aging may be distinguished. Dynamic strain aging (DSA) takes place mainly during intensive plastic forming, or during deformation at elevated temperatures [8]. Static strain aging (SSA) is a process that typically takes place over a longer period of time, subsequent to the plastic deformation. In the case of the wires mentioned above, SSA plays an important role, as it significantly effects their tensile properties.

A comprehensive kinetic model for SSA was proposed by Cottrell and Bilby [5]. This model was later modified by Harper, who obtained

$$W = 1 - \exp \left[-3L \left(\frac{\pi}{2} \right)^{\frac{1}{3}} \left(\frac{ADt}{kT} \right)^{\frac{2}{3}} \right], \quad (1)$$

where W is the amount of interstitial solute that segregates to the dislocations in time t , L is the dislocation density, D is the diffusion coefficient, k the Boltzmann constant and A is a constant that characterizes the interaction between the interstitial atoms and the dislocations [9]. For low-carbon steels, Harper's model is considered conceptually correct. Nevertheless, several of its limitations have been highlighted. Most importantly, it loses its validity as the aging process progresses, where back diffusion and saturation effects take place [10–14].

For high-carbon steels, especially when the entire process is described until saturation, the more general Johnson–Mehl–Avrami–Kolmogorov (JMAK) equation is widely used:

$$F = 1 - \exp[-(Bt)^n], \quad (2)$$

where F is the transformed fraction, B is the rate constant, t is time and n is the time exponent [7,15–20].

The interpretation of the transformed fraction in the case of homogenous transformations is not as obvious as in the case of phase transition processes with nucleation and growth. However, this term is commonly used in general if the progress of the transformation can be characterized by a monotonous change in given physical parameters [21]. In the case of strain aging, examples of such parameters may be the yield strength or the elongation [20]. Thus, the F transformed fraction at a given time can be interpreted as the ratio of the change that takes place until then, and the total change of the parameter

until the process is completed. This definition is widely used for kinetic analyses and simulations of homogenous as well as heterogenous transformations [22].

Microstructure and its potential variation also influence the aging process. This can be generally taken into consideration through its impact on the carbon diffusion [23]. Diffusion is strongly affected by temperature, which is taken into consideration through the Arrhenius-type temperature dependence of B [24,25]. High temperature enhances the diffusion rate of the carbon atoms; hence, strain aging becomes faster at elevated temperatures [26]. It is discussed in the literature that above 200 °C iron-carbide decomposition, which results in excess interstitial carbon, also affects the rate of strain aging [27].

At elevated temperatures, other processes may take place, such as phase transformation and high-temperature corrosion. The significance of the role these mechanisms may play in the case of the investigated hose reinforcement materials is determined by the actual temperature the wires and cables see during the manufacturing or the operation of the rubber hoses. The upper limit of the mentioned temperature is between 100 °C and 180 °C [1]. Hence, within the scope of the present paper, SSA is studied up to 200 °C.

One of the processes with considerable impact on mechanical properties of steels is the annealing, which involves recrystallization [28,29]. Nevertheless, annealing mainly takes place in high-carbon steels at temperatures higher than the vulcanization or the operational temperature of the flexible pipes. Thus, its influence is not significant in the case of wires and cords in the investigated temperature range below 200 °C [30].

Unlike annealing, high-temperature corrosion may take place even under 200 °C if sufficiently long heat aging was applied. The influence of this phenomenon is not considered in this study, as all the examined wires are brass- or zinc-coated, which effectively protects the steel surface from corrosion [31].

During both the extensive deformation and the isothermal holding periods, the microstructure is changing. Comprehensive studies have pointed out that during heavy drawing, the carbide lamellae of the pearlite dissolve [32–34]. The dissolved carbon partially precipitates during the low-temperature aging. Microstructural changes other than this are generally considered to have limited relevance when SSA is investigated in the low temperature range ($T < 200$ °C) [35–37].

The degree of plastic deformation affects the actual dislocation density [38,39]. Hence, it has a significant impact on the strain aging process as well. The kinetics of strain aging are considerably influenced by alloying and carbon content. Based on the special role of carbon atoms, the effect of carbon content is trivial. Nevertheless, other elements differ in their effect on carbon solubility and carbon diffusion [40]. Therefore, the chemical composition of steel is important in the study of strain aging.

Thin wire ropes built into the structure of rubber hoses are exposed to a vulcanization procedure at around 150 °C. This temperature is high enough to start SSA of the steel wires. In some cases, depending on the duration of the procedure, SSA can even be totally completed. Thus, the most important mechanical parameters of the wire ropes are also modified. Due to the SSA effect, the tensile strength of wires—just as of the whole steel cord—increases, while their strain capacity decreases.

It is a basic requirement for the high-strength stranded structures that the component wires can work together during the application, especially under tension [3]. The homogeneity of load distribution over the wires can be ensured by minimizing the variation in strength and elongation. This can usually be evaluated before the steel cord is built in the rubber hose, so well before the inevitable heat treatment of the vulcanization process takes place. Some of the most relevant questions include how significant is the change that occurs in the material properties during the heat treatment, and are the changes mainly uniform or do they vary from wire to wire. These are of special interest in the case of steel cords composed of wires with significantly different diameters. To study the effect in time, kinetic analysis of SSA is needed. Moreover, how SSA affects the damage and failure mode of the stranded structures is also an important question.

The intention of this study is to answer the questions raised above. High-strength steel wires and two types of steel strands are investigated. The wires are made of high-carbon steel with a specific diameter, chemical composition and strength. The two types of strands represent the Warrington and compact structures. Both are specifically used as primary reinforcement materials for high-pressure oil and gas hoses. The extent of the change in material characteristics of the single wires due to the SSA effect is examined as a function of time and temperature. In this study, the tensile properties of the materials are investigated in detail. Although SSA impact, for instance on the torsional or bending properties of wires, is also significant, in the mentioned special application, the axial tensile characteristics are much more relevant [41]. The JMAK model is used for comprehensive kinetic analysis of the process. Furthermore, quantitative results are presented for the magnitude of SSA impact on the steel cord tensile properties. Based on these appropriate parameters for the cord as well as the whole, flexible pipe designs are suggested.

In addition, an irregular failure mode of Warrington-type strands is revealed. This premature fracture is proven to take place due to SSA. The damage mechanism is investigated and fundamentally explained. Engineering consequences and some areas of possible developments are discussed.

The design method of the steel cords can be improved based on the presented kinetic analysis of the wires. Such methods may take into consideration the SSA-driven change in the material characteristics of wires when the stranding parameters are defined. Therefore, an improved behavior of rubber hose-reinforcing steel cords can be ensured by taking into account the impact of the vulcanization process.

2. Materials and Methods

Commercial-grade cold-drawn high-strength high-carbon steel wires and steel cords made from them were investigated. The chemical composition of the wires can be seen in Table 1.

Table 1. Chemical analysis of the wire steel (wt.%).

Wire Type	C	Mn	Si	P	S
Ø0.71; Ø0.76	0.83	0.53	0.35	0.008	0.009
Ø0.68; Ø0.91	0.88	0.57	0.21	0.009	0.008

The patented and coated semi-finished wires of 2.5 mm diameter were subjected to wet drawing, using oil-based emulsion lubricant in a fine drawing machine. The cold drawing was carried out in 14 steps, resulting in an ultimate relative reduction of 86–92% and final drawing speed of 35 m/s.

Nominal yield strength at 0.2% plastic strain offset ($R_{p0.2}$) and coating type of the wires are given in Table 2.

Table 2. Nominal diameter, yield strength and coating type of the wires.

Diameter (mm)	$R_{p0.2}$ (N/mm ²)	Coating
Ø0.71	1960	67% Cu/33% Zn
Ø0.76	1760	67% Cu/33% Zn
Ø0.68	1960	Zn
Ø0.91	1760	Zn

Two types of steel cords composed of these wires were examined, with cord diameters of 3.6 mm and 4.5 mm (Table 3). The relatively simple structure of Ø3.6C cord represents the class of compact strands mainly constructed from equal filaments. The more complex Ø4.5W cord falls into the category of Warrington cords. Both types of cords are mostly used as main reinforcements of high-pressure oil and gas rubber hoses.

Table 3. Nominal maximum force, lay length and structure of steel cords.

Cord Type	F_{\max} (N)	LL (mm)	Structure
Ø3.6C	18,000	37	$1 \times \text{Ø}0.76 + 6 \times \text{Ø}0.71 + 12 \times \text{Ø}0.71$
Ø4.5W	27,000	45	$3 \times \text{Ø}0.68 + 7 \times \text{Ø}0.91 + (7 \times \text{Ø}0.68 + 7 \times \text{Ø}0.91)$

Samples of Ø0.71 wire for kinetic investigation were artificially aged in an electrically heated laboratory oven with spiral way forced hot air circulation at temperatures of 80, 100, 125, 150, 180 and 200 °C. Continuous air ventilation ensured temperature control with an accuracy of ± 1 °C with transient periods less than 10 s. After the specimens were removed from the oven, they were instantly quenched in water at 0 °C. At each temperature, a minimum of six different aging periods were applied from 3 min to 729 min. For temperatures 80–125 °C, additional heat treatment periods were added up to 59,049 min in order to investigate the SSA process all over its transient course. Specimens in as-drawn conditions were also retained as control groups. All samples were taken from the same drawing batch and stored for no longer than 30 days before preparation and testing. The storage temperature was kept below 10 °C to mitigate the impact of any unintended early aging.

In order to gain quantitative information about the impact of SSA on the mechanical parameters, steel cord specimens from both Ø3.6C and Ø4.5W types were heat treated at 150 °C for 45 min. The number of samples used for the measurements were 315 and 76, respectively, with the same numbers of pieces kept intact as control groups.

Load–elongation curves were determined via tensile testing at room temperature at a constant load rate of 40 N/s. A universal tensile testing machine with electromechanical drive and full software control was used for tensile testing. The machine was equipped with a capstan grip system, and its measuring range was 0–50 kN. Elongation was measured with an optical extensometer. Maximum force (F_{\max}), force at yield—taken at 0.2% plastic strain offset—(F_{02}), total elongation at break (ϵ) and its purely plastic component (ϵ_p) were evaluated. It is noted that in the case of the investigated high-strength materials, F_{\max} is the same as the force at break. Characterizing steel wires, ultimate tensile strength (R_m) and proof stress (R_{p02}) are more conventional; thus, they are calculated from the directly measured relevant forces F_{\max} and F_{02} respectively.

3. Results and Discussion

3.1. Character of Static Strain Aging Effect on Wires

The yield strength of Ø0.71 wire is determined after isothermal aging at temperature levels in the 80–200 °C range (Figure 2). The length of the applied heat treatment periods are exponentially extended starting from 3 min. Each dot in Figure 2 represents the mean value of three independent measurements.

Yield strength was also determined in as-drawn conditions. The mean value of R_{p02} without heat treatment is 2292 N/mm².

A significant and generally steady increase is found in R_{p02} as the aging time is prolonged at each treatment temperature. The tendency becomes sharper as the aging temperature is raised. The saturation character of the trend is obvious above 100 °C as R_{p02} attains maximum in the 2570–2650 N/mm² interval from the initial average value of 2300 N/mm². Under 80–100 °C aging conditions, the same effect is presumable.

The exact same process character is found for R_m with an initial value of 2540 N/mm², which is gradually rising and finally stabilizes in the 2640–2680 N/mm² range. This presents a total change of R_m caused by SSA around one-third that can be seen for R_{p02} .

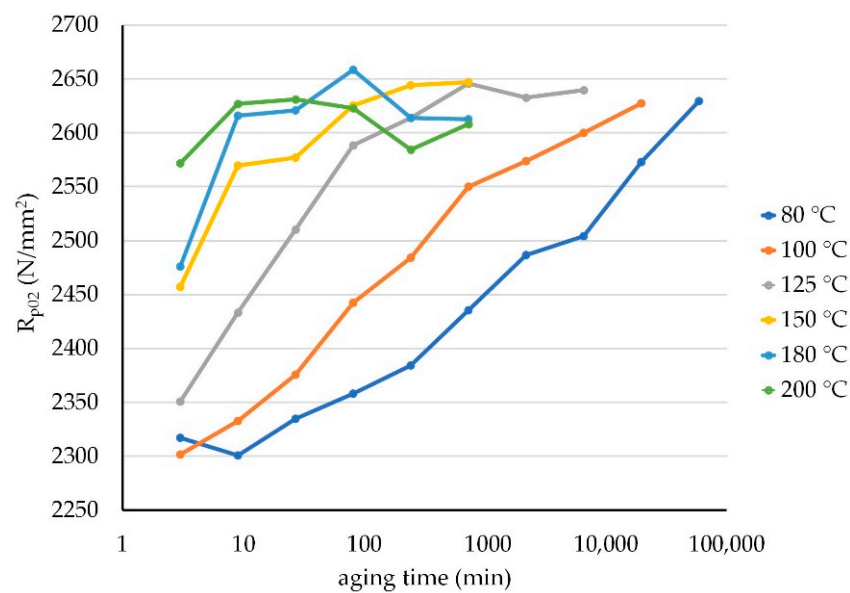


Figure 2. Yield strength vs. aging time ($\text{Ø}0.71$ wire, 80–200 °C).

From tensile diagrams, total elongation ε is recorded. Then, by simple separation from the linear part, the pure plastic strain ε_p is determined. As opposed to the steady increase in strength, monotonous decline is observed as the treatment time prolongs in the cases of all of the aging temperatures previously applied (Figure 3). Stabilization of plastic strain capacity of the material is apparent for aging temperatures of 125–200 °C. Ultimate ε_p values are as low as 0.2–0.25%. Just like in the case of the strength properties, this remains to be proven for aging conditions at or below 100 °C. Nevertheless, plummeting from an original 0.7% figure makes overall plastic strain the parameter that is particularly affected by SSA. The difference between final R_{p02} and R_m values is almost negligible, which matches the minimal ε_p value found after long-term heat treatment.

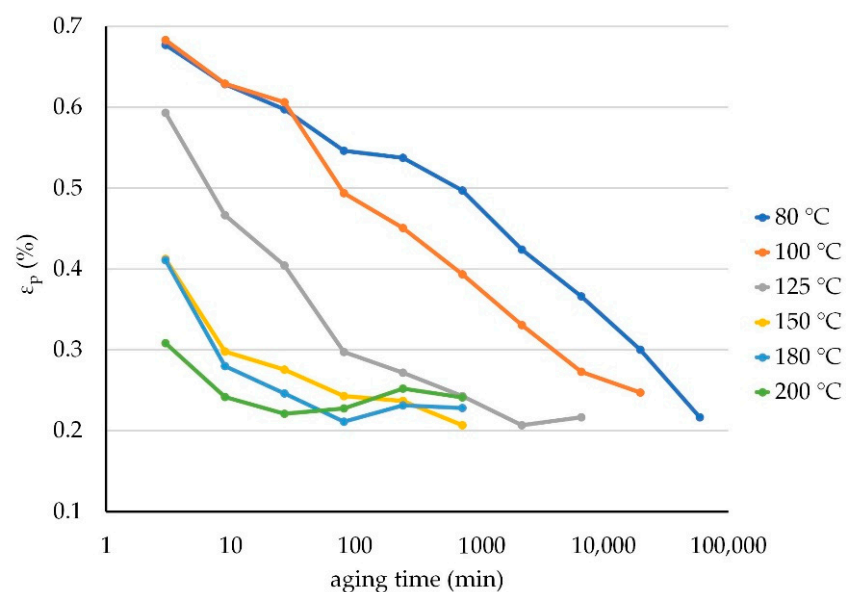


Figure 3. Plastic strain vs. aging time ($\text{Ø}0.71$ wire, 80–200 °C).

3.2. Kinetic Analysis

Based on the complete set of experimental data, time- and temperature-dependence of SSA are investigated in detail by means of the JMAK kinetic model applied for the R_{p02} proof stress values.

In this case, the transformed fraction F is given by

$$F = \frac{R_{p02}^t - R_{p02}^0}{R_{p02}^{\max} - R_{p02}^0}, \quad (3)$$

where R_{p02}^t is the proof stress measured after a heat treatment time of t , R_{p02}^0 the same parameter taken in as-drawn condition and R_{p02}^{\max} is the maximum proof stress value [42].

In the case of low temperatures of 80–100 °C, data from short-period aging that result in F less than 2.5% are filtered out from the examined set. In the case of long-period aging at high temperatures of 180–200 °C, data representing the state well beyond saturation are neglected as well. In this manner, the numerical information of SSA kinetics contained by the remaining data set was significantly larger than the order of the measurement error.

JMAK plots can be seen in Figure 4.

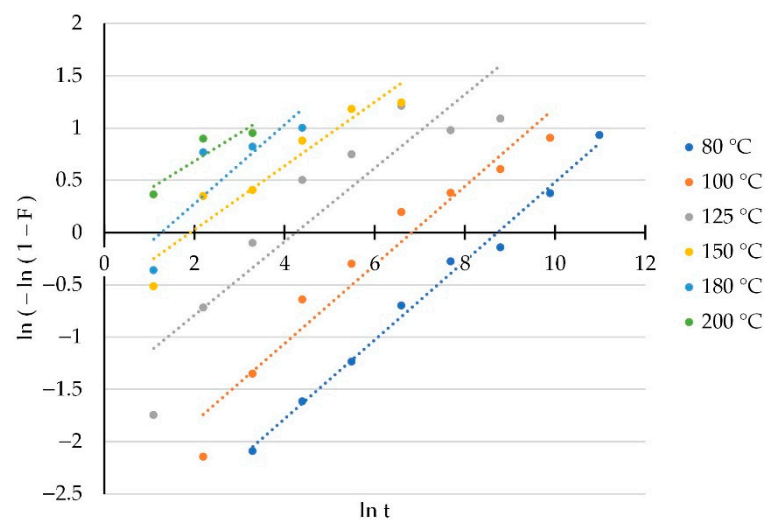


Figure 4. Johnson-Mehl-Avrami-Kolmogorov plots of proof stress (Ø0.71 wire, 80–200 °C).

The plots that belong to different temperatures are separated, and the goodness of the plot linearization is satisfactory, taking into consideration that the applied model is mathematically relatively simple.

Time exponents and rate constants are presented in Table 4. It is found that the variation of the n values with temperature is limited, so universal use of their mean value $n_{\text{avg}} = 0.343$ is reasonably proposed within the temperature range of 80–200 °C.

Table 4. Aging temperatures, the corresponding time exponents and rate constants (Ø0.71 wire, 80–200 °C).

T (°C)	80	100	125	150	180	200
n	0.377	0.376	0.352	0.306	0.377	0.267
B (1/s)	2.73×10^{-6}	1.81×10^{-5}	2.39×10^{-4}	2.46×10^{-3}	4.70×10^{-3}	2.93×10^{-2}

The JMAK kinetic model was primarily introduced to describe heterogenous phase transitions [43,44]. Nevertheless, for strain aging, it is commonly used as a generalized form of Harper’s original relation given in Equation (1) [7,20]. The time exponent is sensitive to the geometrical conditions. These conditions are mainly determined by the thin wire and the fine pearlitic structure.

Studies on drawn high-carbon steel wires of larger diameters explain the deviation from the original $2/3$ value by means of the different dislocation distribution. In the case of plastically deformed pearlitic steel, cellular dislocation arrangement was found in contrast with the uniform distribution originally assumed by Cottrell, Bilby and Harper [5,9,45,46].

In the case of cellular distribution, the diffusion flux is considered unidirectional—normal to the cell boundary—and leads to a time exponent value of 1/3 [47].

SSA kinetics have been studied by other authors, by examining their effect on the tensile properties, electrical resistivity and internal friction spectra [7,20]. By these methods, time exponents were found in the range of 0.29–0.56 for cold drawn, high-carbon steel wires with similar chemical composition but significantly larger diameter. Our results, summarized in Table 4, noticeably fall in the lower half of this range, which may represent differences in the drawing procedures, the ultimate wire sizes and strengths, the relative reductions and the related interlamellar distances.

Temperature dependence is given through the Arrhenius equation:

$$B = B_0 e^{\frac{-E_a}{RT}}, \quad (4)$$

where B is the rate constant, T is the absolute temperature, B_0 is the so-called pre-exponential factor, E_a is the apparent activation energy and R is the universal gas constant. The Arrhenius plot can be seen in Figure 5.

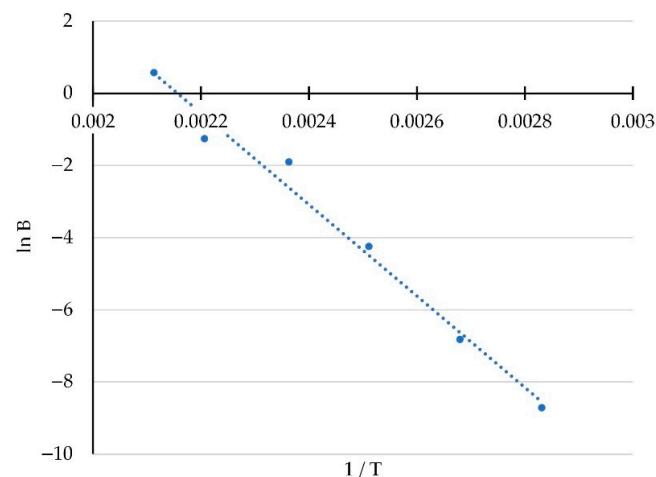


Figure 5. Arrhenius plot ($\varnothing 0.71$ wire, 80–200 °C).

The mean value of the time exponent, the apparent activation energy E_a , the pre-exponential constants A and the correlation coefficient of Arrhenius linearization are given in Table 5.

Table 5. Mean time exponent, apparent activation energy, pre-exponential constant and correlation coefficient of the Arrhenius linearization.

n_{avg}	E_a (kJ/mol)	A (1/s)	R^2
0.343	105.4	1.265×10^{10}	0.984

The goodness of the Arrhenius fit is obvious. The activation energy is in good agreement with those obtained by other authors [7,20,48]. The apparent activation energy highly depends on the diffusivity of the interstitial carbon atoms. Therefore, it characterizes the temperature dependence of the aging process.

Based on the given kinetic analysis in the case of isotherm heat treatment, the variation in the tensile properties of wires can be calculated. Moreover, the mechanical parameters of the stranded cords under service conditions can also be predicted.

3.3. Quantitative Investigation of SSA Effect on Compact Steel Cords with Large Number of Samples

For a quantitative description of the change in the relevant mechanical parameters, $\varnothing 3.6C$ compact-type steel cord is investigated with 630 pieces of samples used for the

measurements. Due to the fact that Ø3.6C consists of nearly the same type of wires, general conclusions can be directly linked to the material of the base filament.

Half of the specimens were tensile tested in untreated conditions, with the other half tested being previously subjected to aging at 150 °C for 45 min. Based on the findings discussed in the preceding subsections, it is considered that SSA has concluded to a significant extent in case of the treated half of the sample. In this manner, results displayed in Table 6 describe the total change in the given material parameters and the related standard deviation (SD) as the aging effect takes place and ultimately reaches stabilized saturation.

Table 6. Strength and strain parameters of Ø3.6C compact steel cord in untreated and aged conditions.

Condition	Mean/SD	$F_{0.2}$ (N)	F_{max} (N)	ϵ (%)	ϵ_p (%)
untreated	mean	16,655	18,735	2.591	1.168
	SD	409	209	0.128	0.131
aged *	mean	19,598	20,095	1.845	0.379
	SD	323	220	0.061	0.063

* 150 °C/45 min.

In the case of steel cord reinforced rubber hoses—the main application area of the examined cords—the vulcanization temperature is typically around 150 °C. For this reason, the effect of SSA phenomenon is of special interest in this condition.

Mean strength and its modification correlate very well with the values gained from measurements on the filaments that were introduced in the previous subsections. This fact confirms the relevancy of results derived from the examination of these simple steel cords for the base wire materials. The accuracy of the measurements is reflected in standard deviation magnitudes below 2.5%.

The falling tendency in elongation with increasing aging time is also associated with the discussed kinetics of SSA of wires. Nevertheless, in the case of Ø3.6C compact steel cord, the average ϵ_p is approximately two times greater than in the case of its Ø0.71 component wire. The same ratio is found both in untreated as well as in aged conditions. This may originate in the well-known structural elongation of cords that affects strain properties under axial loading in addition to the homogenous deformation of the base material [2].

Histograms are used to visualize the data of aged and basic conditions in terms of $F_{0.2}$ and F_{max} in Figure 6, as well as ϵ and ϵ_p in Figure 7.

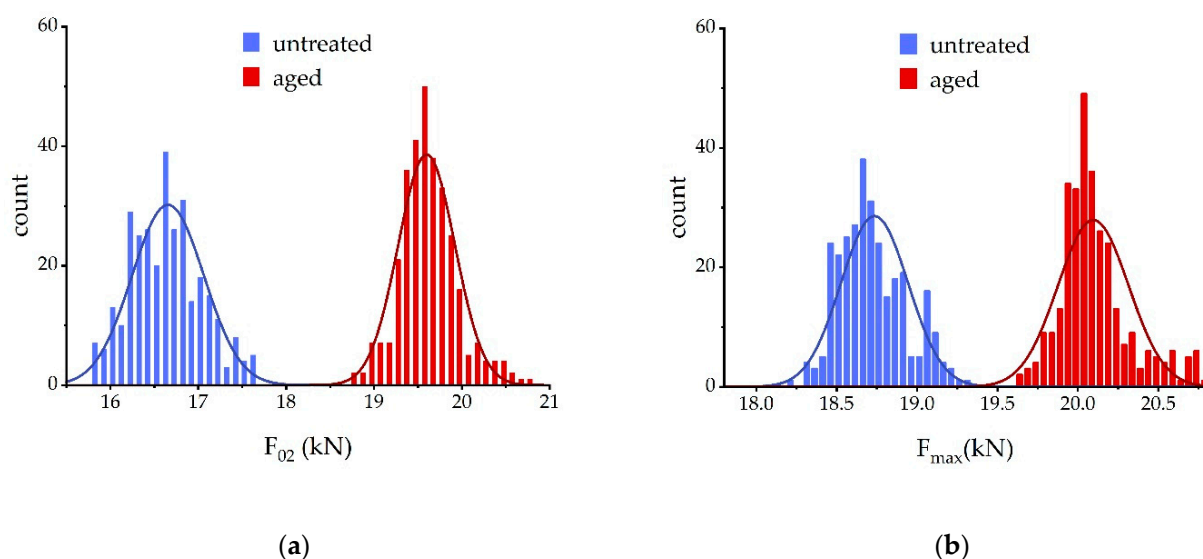


Figure 6. Histograms of (a) force at yield and (b) maximum force for Ø3.6C compact steel cord in untreated and 150 °C/45 min aged conditions.

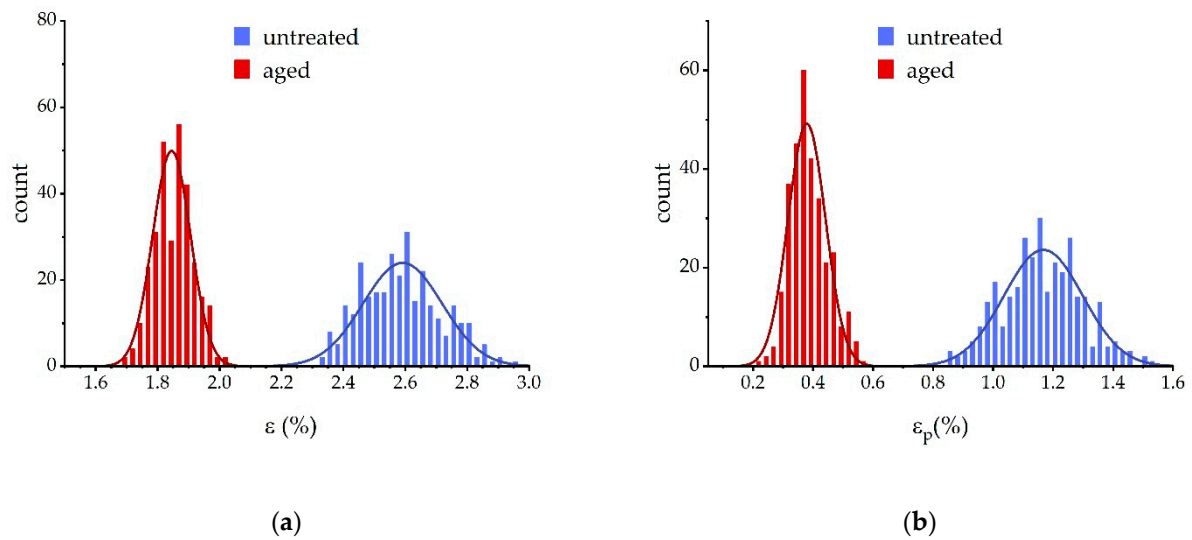


Figure 7. Histograms of (a) total strain at break and (b) plastic strain at break for Ø3.6C compact steel cord in untreated and 150 °C/45 min aged conditions.

Populations of untreated and aged samples are obviously separated, and distributions can be very well approximated by Gaussians. Function parameters can be found in Table 6, where the SD is the square root of the actual variance.

Noticeable differences in distribution profiles are found as the total elongation is compared to the plastic elongation. In theory, if the elastic modulus was not affected by aging, the mentioned profile shape would match more precisely. In addition to measurement inaccuracy, the observed deviation may be caused by a slight variation in Young's moduli caused by SSA.

3.4. Abnormal Sequential Break of Warrington Steel Cords

Force–strain diagrams of Ø3.6C compact and Ø4.5W Warrington cords are recorded. Diagrams taken without heat treatment and subsequent to a 45-min isothermal aging at 150 °C are compared (Figure 8).

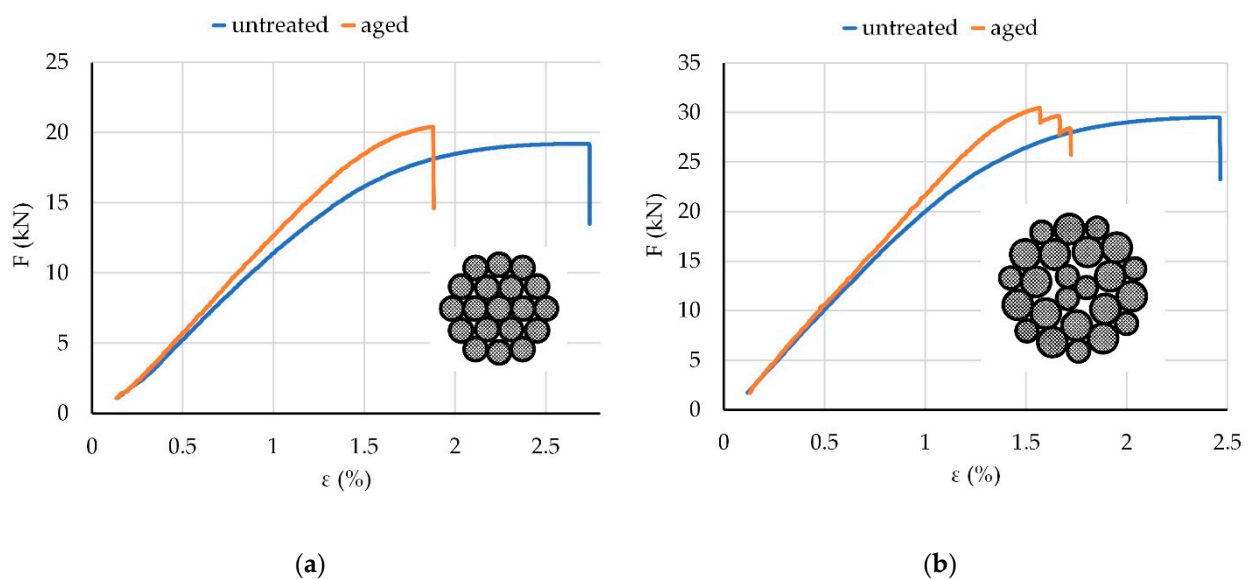


Figure 8. Typical tensile diagrams in untreated and 150 °C/45-min aged conditions of (a) Ø3.6C compact-type steel cord and (b) Ø4.5W Warrington-type steel cord.

Typical tensile curve pairs of a Ø3.6C specimen can be seen in Figure 6a. The overall change in the main mechanical properties discussed in previous subsections is apparent. Moreover, a definite breaking point is observed even in aged conditions, which indicates that all of the wire components of the strand reach their strain capacity limits at the same time. In other words, the properly balanced load distribution over the individual wire filaments—of mostly the same thickness—remained perfect even if SSA took place. Altogether, 315 aged and 315 untreated specimens were used for the tests, and all of them provided the same favorably regular failure mode.

On the other hand, in the case of Ø4.5W Warrington-type steel cords, an irregular break is noticed as the tensile test is performed on previously heat-aged pieces (Figure 6b). Out of the tested 76 aged cord specimens, 68.4% presented sequential pre-mature failure, without such occurrences in the untreated 76-element control group.

The aforesaid uncertain load carrying capacity in the inelastic deformation regime is especially disadvantageous in the case of the given high-pressure oil hose reinforcement steel cords. Those flexible pressure vessels contain numerous concentric helically wound steel cord layers with precisely optimized individual lay angles [1]. Cord orientations are accurately calculated in order to reach proper transmission of the loads between the adjacent reinforcement layers. Due to the significant risk level present in the oil and gas industry, flexible pipe-related standards specify high design safety factors. So, to fulfill these requirements, it is conventional that, in addition to the linearly elastic range, the plastic load-carrying capacity of the steel plies is also utilized as the minimum burst pressure is calculated. Evidently, the revealed adverse failure mode was well below the expected total ply strain and that can have serious consequences if the phenomenon is not handled appropriately.

The anomaly is only experienced in the case of Warrington-type steel cords. This relatively complex structure comprises 10 plies of Ø0.68 wires and 14 plies of Ø0.91 wires. It is considered that the early sequential break is caused by the different aging mechanism of the component wires. Hence, they are investigated in terms of strength and elongation at break in untreated and 150 °C/45-min aged conditions. Results can be seen in Table 7.

Table 7. Mean maximum force and total strain values of Ø0.68 and Ø0.91 wires in untreated and aged conditions.

Wire Type	Condition	F _{max} (N)	ε (%)
Ø0.68	raw	927	2.28
	aged *	1011	1.82
Ø0.91	raw	1424	2.30
	aged *	1545	1.70

* 150 °C/45 min.

Ultimate elongation at break of Ø0.91 wires is found to be 0.1% lower than that of Ø0.68 wires. The irregular failure of the Warrington cord that experienced SSA is explained using the following fundamental hypothesis.

A few of the Ø0.91 wires—those with coincidentally the lowest strain capacity in the aged state—reach their strain limit and get overloaded one by one. Meanwhile, the remaining cord structure—especially the 10 plies of Ø0.68 wires—are still well below its tensile capacity in terms of overall tensile stress as well as the actual strain.

This hypothesis is confirmed since all the drop sequences in force—similarly, as it is displayed in Figure 6b—are found to be in the magnitude of 1500 N, similar to the value of the mean F_{max} of Ø0.91 wires displayed in Table 3.

It is obvious that the cord strength is irreversibly reduced due to the prematurely broken filaments. Furthermore, the sudden loss of balance results in an uncontrolled deformation of the complex strand structure. These two effects ultimately cause rapid failure of the Warrington steel cord well below its theoretical F_{max}.

On one hand, considering the given anomaly, utilizing compact type steel cords in multi-layer high-pressure rubber hoses may be preferable. On the other hand, some resolutions may also be feasible to improve the Warrington steel cords, even with the presently used high-carbon steel grade. Such options may focus on optimization of the cord geometry or alternatively on the wire drawing procedure.

By adjusting the lay angles of wires or modifying the layer structure and number of filaments in the strands, the so-called structural elongation of the cord can be regulated. A design method for this that takes into consideration the impact of SSA and the related change in the strain capacity of the wire material—as it is described in detail above—is recommended.

As an alternative approach for a given strand geometry, the strain properties of the component wires can be varied through the series of the reductions applied during the cold drawing process. In this case, the eventual elongation at yield as well as the elongation at break values must be verified after a heat treatment that is sufficient to complete the SSA at the desired working temperature of the steel cord.

4. Conclusions

The saturation character of SSA on the investigated high-carbon steel wires has been verified in the temperature range of 125–200 °C.

At the typical vulcanization temperature of 150 °C, it has been demonstrated that the material properties after heat aging for 45 min reasonably represents the eventual aged condition of the steel wire. The magnitude of the further change that may be caused by the prolongation of the isothermal heat treatment remains well below the standard deviation of the measured values. This has been confirmed both in terms of and elongation parameters.

Strength and strain values have been determined as a function of the treatment time within the 80–200 °C temperature interval. Based on the obtained data set, the kinetic analysis of SSA has been carried out. The Johnson–Mehl–Avrami–Kolmogorov kinetic model has been fit with satisfactory goodness. The related time exponent is found to fall in the range 0.267–0.377. The impact of aging temperature has been appropriately characterized using the Arrhenius relation. The obtained apparent activation energy is 105.4 kJ/mol.

Quantitative results have been presented for the investigated compact type high-pressure rubber hose reinforcement steel cord. Data have been given based on statistics of a 630-element sample. The SSA effects on the most important mechanical characteristics of the plies have been precisely described. A significant rise in force at yield and maximum force has been found along with a drastic plummeting of the strain capacity in the plastic regime.

The premature sequential failure mode of Warrington-type steel cords was revealed as SSA took place. A fundamental explanation of this unfavorable irregular break has been given based on the different characteristics of SSA in the case of the steel wire components that comprise the Warrington-type cords.

Severe consequences to engineering applications have been discussed. Some potential resolutions have been highlighted that may solve the reported technical anomaly.

Author Contributions: Conceptualization, T.B.M. and P.B.; methodology, P.B. and T.B.M.; formal analysis, T.B.M.; investigation, T.B.M.; data curation, T.B.M.; writing—original draft preparation, T.B.M.; writing—review and editing, P.B.; supervision, P.B. All authors have read and agreed to the published version of the manuscript.

Funding: This research received no external funding.

Institutional Review Board Statement: Not applicable.

Informed Consent Statement: Not applicable.

Data Availability Statement: The data supporting reported results in this study are openly available in FigShare at [<https://doi.org/10.6084/m9.figshare.16699432.v1>] (29 September 2021).

Conflicts of Interest: The authors declare no conflict of interest.

References

1. Bai, Q.; Bai, Y.; Ruan, W. Bonded flexible pipes. In *Advances in Pipes and Pipelines Flexible Pipes*, 1st ed.; John Wiley & Sons, Inc.: Hoboken, NJ, USA, 2017; pp. 357–392.
2. Feyrer, K. *Wire Ropes*, 2nd ed.; Springer: Berlin/Heidelberg, Germany, 2015; pp. 1–58.
3. Costello, G.A. *Theory of Wire Rope*, 2nd ed.; Springer: New York, NY, USA, 1997; pp. 11–43.
4. Bauschinger, J. Variations in the elastic limit of iron and steel. *J. Iron Steel Inst.* **1887**, *1*, 442–444.
5. Cottrell, A.H.; Bilby, B.A. Dislocation theory of yielding and strain aging of iron. *Proc. Phys. Soc.* **1949**, *62A*, 49–61. [[CrossRef](#)]
6. Parvin, H.; Kazeminezhad, M. Development a dislocation density based model considering the effect of stacking fault energy: Severe plastic deformation. *Comput. Mater. Sci.* **2014**, *95*, 250–255. [[CrossRef](#)]
7. Kemp, I.P.; Pollard, G.; Bramley, A.N. Static strain aging in high carbon steel wire. *Mater. Sci. Technol.* **1990**, *6*, 331–337. [[CrossRef](#)]
8. Staiger, M.P.; Brownrigg, A.; Hodgson, P.D.; Davies, C.H.J. Multistage strain aging of low-carbon steels. *Mater. Sci. Eng. A* **2004**, *364*, 35–47. [[CrossRef](#)]
9. Harper, S. Precipitation of Carbon and Nitrogen in Cold-Worked Alpha-Iron. *Phys. Rev.* **1951**, *83*, 709–712. [[CrossRef](#)]
10. Kamber, K.; Keefer, D.; Wert, C. Interaction of interstitials with dislocations in iron. *Acta Metall.* **1961**, *9*, 403–414. [[CrossRef](#)]
11. Ham, F.S. Stress-assisted precipitation on dislocations. *J. Appl. Phys.* **1959**, *30*, 915–926. [[CrossRef](#)]
12. De, A.K.; Vandeputte, S.; De Cooman, B.C. Kinetics of strain aging in Bake hardening ultra low carbon steel—a comparison with low carbon steel. *J. Mater. Eng.* **2001**, *10*, 567–575. [[CrossRef](#)]
13. Bullough, R.; Newman, R.C. The kinetics of migration of point defects to dislocations. *Rep. Prog. Phys.* **1970**, *33*, 101–148. [[CrossRef](#)]
14. Baird, J.D. Strain aging of steel a critical review. *Iron Steel* **1963**, *36*, 368–374.
15. Avrami, M. Kinetics of phase change I. General Theory. *J. Chem. Phys.* **1939**, *7*, 1103–1112. [[CrossRef](#)]
16. Avrami, M. Kinetics of phase change II. Transformation. *J. Chem. Phys.* **1940**, *8*, 212–224. [[CrossRef](#)]
17. Avrami, M. Kinetics of phase change III. Microstructure. *J. Chem. Phys.* **1941**, *9*, 177–184. [[CrossRef](#)]
18. Johnson, W.A.; Mehl, R.F. Reaction kinetics in processes of nucleation and growth. *Trans. Am. Inst. Min. Met. Eng.* **1939**, *195*, 416–422.
19. Kolmogorov, A.N. On the statistical theory of crystallization of metals. *Izv. Akad. Nauk SSSR Ser. Mat.* **1937**, *1*, 355–359.
20. Buono, V.T.L.; Andrade, M.S.; Gonzalez, B.M. Kinetics of strain aging in drawn pearlitic steels. *Metall. Mater. Trans.* **1998**, *29A*, 1415–1423. [[CrossRef](#)]
21. Lamontagne, A.; Massardier, V.; Sauvage, X.; Kléber, X.; Mari, D. Evolution of carbon distribution and mechanical properties during the static strain ageing of heavily drawn pearlitic steel wires. *Mater. Sci. Eng. A* **2016**, *667*, 115–124. [[CrossRef](#)]
22. Gyöngyösi, S.; Tóth, A.; Barkóczy, P. Simulation of Phase Transformations Driven by Short Range Diffusion by Cellular Automaton. *Mater. Sci. Forum* **2010**, *659*, 405–410. [[CrossRef](#)]
23. Takahashi, J.; Kosaka, M.; Kawakami, K.; Tarui, T. Change in carbon state by low-temperature aging in heavily drawn pearlitic steel wires. *Acta Mater.* **2012**, *60*, 387–395. [[CrossRef](#)]
24. Criado, J.M.; Ortega, A. Non-isothermal crystallization kinetics of metal glasses: Simultaneous determination of both the activation energy and the exponent n of the JMA kinetic law. *Acta Metall.* **1987**, *35*, 1715–1721. [[CrossRef](#)]
25. Woldt, E. The relationship between isothermal and non-isothermal description of Johnson-Mehl-Avrami-Kolmogorov kinetics. *J. Phys. Chem. Solids* **1992**, *53*, 521–527. [[CrossRef](#)]
26. Veiga, R.G.A.; Perez, M.; Becquart, C.S.; Domain, C. Atomistic modeling of carbon Cottrell atmospheres in BCC iron. *J. Phys. Condens. Matter* **2013**, *25*, 025401. [[CrossRef](#)] [[PubMed](#)]
27. Nishimo, K.; Takahashi, K. Strain age hardening in range 150–350 °C of carbon steel. *Trans. Jpn. Inst. Metals* **1962**, *3*, 57–62. [[CrossRef](#)]
28. Handa, K.; Kimura, Y.; Yasumoto, Y.; Kamioka, T.; Mishima, Y. Effect of deformation and annealing temperatures on ultrafine microstructure development and yield strength of pearlitic steel through continuous recrystallization. *Mater. Sci. Eng. A* **2010**, *527*, 1926–1932. [[CrossRef](#)]
29. Jafari, M.; Bang, C.W.; Han, J.C.; Kim, K.M.; Na, S.H.; Park, C.G.; Lee, B.J. Evolution of microstructure and tensile properties of cold-drawn hyper-eutectoid steel wires during post-deformation annealing. *J. Mater. Sci. Technol.* **2020**, *41*, 1–11. [[CrossRef](#)]
30. Xiang, L.; Liang, L.W.; Wang, Y.J.; Chen, Y.; Wang, H.Y.; Dai, L.H. One-step annealing optimizes strength-ductility trade-off in pearlitic steel wires. *Mater. Sci. Eng. A* **2019**, *757*, 1–13. [[CrossRef](#)]
31. Romaine, A.; Crozet, M.; Mary, N.; Normand, B.; Chassagne, M.; Dufour, F. Importance of the surface and environmental conditions on the corrosion behavior of brass, steel and brass coated steel wires and brass coated steel cords. *Corros. Sci.* **2020**, *177*, 108966. [[CrossRef](#)]
32. Feng, H.; Cai, L.; Wang, L.; Zhang, X.; Fang, F. Microstructure and strength in ultrastrong cold-drawn medium carbon steel. *J. Mater. Sci. Technol.* **2021**, *97*, 89–100. [[CrossRef](#)]
33. Zhou, L.; Fang, F.; Zhou, J.; Xie, Z.; Jiang, J. Strain-induced coarsening of ferrite lamella in cold drawn pearlitic steel wire. *Mater. Sci. Eng. A* **2020**, *771*, 138602. [[CrossRef](#)]

34. Zhou, Y.T.; Shao, X.H.; Zheng, S.J.; Ma, X.L. Structure evolution of the Fe₃C/Fe interface mediated by cementite decomposition in cold-deformed pearlitic steel wires. *Mater. Sci. Technol.* **2022**, *101*, 28–36. [[CrossRef](#)]
35. Wei, D.; Li, L.; Min, X.; Fang, F.; Xie, Z.; Jiang, J. Microstructure and mechanical properties of heavily cold drawn pearlitic steel wires: Effects of low temperature annealing. *Mater. Charact.* **2019**, *153*, 108–114. [[CrossRef](#)]
36. Wei, D.; Min, X.; Hu, X.; Xie, Z.; Fang, F. Microstructure and mechanical properties of cold drawn pearlitic steel wires: Effects of drawing-induced heating. *Mater. Sci. Eng. A* **2020**, *784*, 139341. [[CrossRef](#)]
37. Gondo, S.; Tanemura, R.; Mitsui, R.; Kajino, S.; Asakawa, M.; Takemoto, K.; Tashima, K.; Suzuki, S. Relationship between mesoscale structure and ductility of drawn high carbon steel wire. *Mater. Sci. Eng. A* **2021**, *800*, 140283. [[CrossRef](#)]
38. Dunlop, J.W.C.; Brechet, Y.J.M.; Legras, L.; Zurob, H.S. Modelling isothermal and non-isothermal recrystallisation kinetics: Application to Zircaloy-4. *J. Nucl. Mater.* **2007**, *366*, 178–186. [[CrossRef](#)]
39. Pradell, T.; Crespo, D.; Clavaguera, N.; Clavaguera-Mora, M.T. Diffusion controlled grain growth in primary crystallization: Avrami exponents revisited. *J. Phys. Condens. Matter* **1998**, *10*, 3833–3844. [[CrossRef](#)]
40. Davies, N.P.W. Strain Aging in Ultra-High Strength Drawn Pearlitic Steels. Ph.D. Thesis, University of the Witwatersrand, Johannesburg, South Africa, 1987.
41. Suliga, M. The effect of drawing speed on the ageing of high-carbon steel wire. *Arch. Metall. Mater.* **2018**, *4*, 1931–1935.
42. Ahmedabadi, P.M.; Kain, V. Modelling transformation kinetics of different solid-state reactions using sigmoidal model. *Materialia* **2019**, *5*, 100235. [[CrossRef](#)]
43. Benke, M.; Mertinger, V.; Barkoczy, P. Investigation of the kinetic of a bainitic reaction upon heating in a CuAlNiMn and a CuAlNiMnFe shape memory alloy. *Mater. Sci. Forum* **2013**, *752*, 3–9. [[CrossRef](#)]
44. Benke, M.; Tranta, F.; Barkoczy, P.; Mertinger, V.; Daroczi, L. Effects of heat-flux features on the differential scanning calorimetry curve of a thermoelastic martensitic transformation. *Mater. Sci. Eng. A* **2008**, *481–482*, 522–525. [[CrossRef](#)]
45. Embury, J.D.; Fisher, R.M. The structure and properties of drawn pearlite. *Acta Metall.* **1966**, *14*, 147–159. [[CrossRef](#)]
46. Chandhok, V.K.; Kasak, A.; Hirth, J.P. Structures and strengthening mechanisms in carbon steel wire. *Am. Soc. Met. Trans. Quart.* **1966**, *59*, 288–301.
47. Lement, B.S.; Cohen, M. A dislocation-attraction model for the first stage of tempering. *Acta Metall.* **1956**, *4*, 469–476. [[CrossRef](#)]
48. Yamada, Y. Static strain aging of eutectoid carbon steel wires. *Trans. Iron Steel Inst. Jpn.* **1976**, *16*, 417–426. [[CrossRef](#)]